# N-Type polymeric mixed conductors for all-in-one aqueous electrolyte gated photoelectrochemical transistors†

Latifah Almulla, [ID] [a] Victor Druet,[a] Christopher E. Petoukhoff,[b] Wentao Shan,[a] Nisreen Alshehri,[bc] Sophie Griggs,[d] Yazhou Wang,[a] Maryam Alsufyani,[d] Wan Yue, [ID] [e] Iain McCulloch,[bd] Frédéric Laquai [ID] [b] and Sahika Inal [ID] *[a]

An organic photoelectrochemical transistor (OPECT) is an organic electrochemical transistor (OECT) that utilizes light to toggle between ON and OFF states. The current response to light and voltage fluxes in aqueous media renders the OPECT ideal for the development of next-generation bioelectronic devices, including light-assisted biosensors, light-controlled logic gates, and artificial photoreceptors. However, existing OPECT architectures are complex, often requiring photoactive nanostructures prepared through labor-intensive synthetic methods, and despite this complexity, their performance remains limited. In this study, we develop aqueous electrolyte-compatible optoelectronic transistors using a single n-type semiconducting polymer. The n-type film performs multiple tasks: (1) gating the channel, (2) generating a photovoltage in response to light, and (3) coupling and transporting cations and electrons in the channel. We systematically investigate the photoelectrochemical properties of a range of n-type polymeric mixed conductors to understand the material requirements for maximizing phototransistor performance. Our findings contribute to the identification of crucial material and device properties necessary for constructing high-performance OPECTs with simplified design features and a direct interface with biological systems.

## New concepts

An organic photoelectrochemical transistor (OPECT) is an organic electrochemical transistor (OECT), where the output current is controlled by the intensity of light that hits the device. OPECT is not an ordinary phototransistor; it operates in water, and it can have very high gain upon light exposure. However, to render an OECT photosensitive, photoactive materials should be integrated into the device, which, has relied on additional metals, sophisticated nanostructures, and tedious synthetic approaches. In this work, we develop an all-in-one OPECT structure, where a single polymeric mixed ionic–electronic conductor is used as the photoactive gate and the channel material. The device is turned on with light exposure and shows exceptional transconductance values in the presence of light. We study a range of n-type polymeric mixed conductors to understand the material and device requirements that maximize photodetector performance. By systematically investigating various n-type polymers, we uncover a fundamental correlation: longer exciton lifetimes lead to larger photovoltage generation. This OPECT design not only advances water-compatible photodetector technology but also provides critical insights into events that occur at conjugated polymer film/aqueous salt interface upon light exposure, with implications in bioelectronics as well as photocatalysis.

## Introduction

The organic electrochemical transistor (OECT) has emerged as an alternative transducer, outperforming other electrolyte-gated transistors of similar geometry in terms of transconductance ($g_{m}$).[1–3] The OECT uses an organic mixed ionic–electronic conductor, often in the form of conjugated polymers, in the channel between the source and drain electrodes, directly interfacing with an aqueous electrolyte. The gate electrode is immersed in the same electrolyte and connected to the source contact. Applying a voltage at the gate electrode with respect to the source contact ($V_{GS}$) drives electrolyte ions inside the polymeric channel, where they stabilize the electronic charges injected from the drain electrode. The coupling between these ionic and electronic charges across the entire volume of the channel results in a substantial change in the channel current ($I_{DS}$). The large $I_{DS}$ change with respect to a small $V_{GS}$ modulation yields high $g_{m}$

*[a] King Abdullah University of Science and Technology (KAUST), Biological and Environmental Science and Engineering Division, Organic Bioelectronics Laboratory, Thuwal 23955-6900, Saudi Arabia. E-mail: sahika.inal@kaust.edu.sa*

*[b] KAUST Solar Center, Physical Science and Engineering Division, Materials Science and Engineering Program, Thuwal 23955-6900, Saudi Arabia*

*[c] Physics and Astronomy Department, College of Sciences, King Saud University, Riyadh 12372, Saudi Arabia*

*[d] Department of Chemistry, University of Oxford, Oxford, OX1 3TA, UK*

*[e] Guangzhou Key Laboratory of Flexible Electronic Materials and Wearable Devices, School of Materials Science and Engineering, Sun Yat-sen University, Guangzhou 510275, People's Republic of China*

† Electronic supplementary information (ESI) available. See DOI: https://doi.org/10.1039/d4mh00267a

$(g_m = \frac{\partial I_{DS}}{\partial V_{GS}})$ values,[4] allowing to detect small potentiometric signals at the gate electrode. Such signals may arise from biological events such as neuronal activity[5] or protein–protein binding.[6]

The high $g_m$ of OECTs can be instrumental in building powerful light-to-current transducers operating inside aqueous electrolytes, provided that either the channel or the gate electrode consists of a photoactive material. Such a device is called an organic photoelectrochemical transistor (OPECT). OPECTs have been constructed using various photoactive materials, including metal–organic frameworks,[7,8] quantum dots,[9,10] nanoparticles,[11] nanotubes,[12] and azobenzenes,[13] incorporated at the gate electrode. Paired with a channel comprising the conducting polymer poly(3,4-ethylene dioxythiophene)polystyrene sulfonate (PEDOT:PSS), these OPECTs operate in "depletion mode", wherein light exposure of the gate electrode leads to a reduction in PEDOT:PSS channel current. This behavior is undesirable for sensing applications, as any fluctuations in channel current can disrupt sensor data. Moreover, the limited light-triggered change in depletion mode device characteristics due to the lack of a subthreshold region obscures harnessing the high amplification of OECTs.[14]

Additionally, many of these devices rely on soluble electron donors or acceptors, such as ascorbic acid, added to the electrolyte to suppress the recombination of photogenerated electron–hole pairs.[15–17] However, integrating such chemicals into biologically relevant environments can be challenging, potentially interfering with the stability of the channel material and hindering long-term device performance. Furthermore, as the light response often proceeds through a faradaic event (*i.e.*, electron transfer to/from the gate electrode), interpreting calibration curves can be difficult without a reference electrode.[4] Finally, previous studies have primarily focused on reporting changes in channel and gate currents upon illumination for applications such as light-assisted biosensing or neuromorphic devices. The potential of these devices as water-compatible phototransistors remains largely unexplored.

We have recently demonstrated that it is possible to construct an all-in-one, micron-scale OPECT wherein a single n-type polymeric mixed conductor fulfills multiple functions by serving as the photosensitive gate and channel material.[18] Remarkably, despite its simplicity, this device generates a 400-fold increase in channel current in response to red light, with light sensitivities surpassing those of the previously reported OPECTs. This versatile device can serve as a building block for a water-compatible photodetector or a circuit element with a signal-to-noise ratio exceeding what is physically achievable with state-of-the-art OECTs, simply by using light as the input. However, the specific material properties that enable this unique device operation remain unclear, hindering the maximization of light intensity-to-current modulations through materials design.

In this study, we investigate the photoelectrochemical properties of a wide range of n-type polymeric mixed conductors with various backbones and side chains to elucidate the factors governing light interactions with mixed charge transport. Our findings reveal that the response to light at the electrolyte interface remains consistent across n-type polymers, provided the film is in an undoped state prior to illumination. We identify a potentiometric mechanism utilized by all responsive devices to detect light, despite the differences in their photo-detection performance. We evaluate each film's photoresponse ability using cyclic voltammetry, potentiometry, electrochemical impedance spectroscopy, transient absorption, and time-resolved terahertz spectroscopy. We find that a long exciton lifetime is key to enhancing the photovoltage response, while a high intrinsic OECT $g_m$ maximizes the phototransistor figures of merit. These findings offer valuable guidelines for optimizing OPECT performance through materials and device design strategies, with broad applicability to emerging applications such as light-assisted biomarker sensing, bioemission detection, and artificial retina development.

# Experimental section

### Materials

$p(C_6NDI-T)$,[19] P-90,[20] gAIID-2FT,[21] and P-75[22] were synthesized using existing protocols. BBL was purchased from Sigma Aldrich and used as received. $1\times$ PBS electrolyte was prepared according to the instructions provided by the manufacturer (Merck).

### Device preparation

Electrodes and OECTs were fabricated on glass wafers following a standard photolithographic process. Glass wafers were cleaned through immersion in piranha ($H_2O_2 : H_2SO_4$, ratio $1:4$) bath, washed with water, dried under nitrogen ($N_2$), and exposed to oxygen plasma (Nanoplas DSB 6000). A bilayer photoresist composed of LOR 5B (Microchem) and S1813 (Shipley) was spin-coated and exposed to UV light by 6200 mask alignment system to create electrodes and interconnection pads as well as OECT components (channels, gates, pads, and interconnects). The photoresist pattern was generated by MF-319 developer. A 10 nm of Cr and 100 nm of Au layers were deposited using Magnetron sputtering (Equipment Support Company Ltd ESCRD4) and lifted by NMP solvent. A thin layer of Parylene C was vaporized using SCS Labcoater 2 and adhered on the surface with Silane for electrical insulation of interconnects. Another layer of Parylene C, serving as a sacrificial layer for polymer film patterning, was vaporized. A layer of AZ9260 was spin-coated and developed through the AZ developer as a mask for reactive ion etching (Oxford Instruments Plasmalab 100-ICP 380). The resulting Au electrodes had an area of $500 \times 500\ \mu m^2$ while the OECT gate and channel had an area of $500 \times 500\ \mu m^2$ and $10 \times 100\ \mu m^2$, respectively.

The solutions of n-type polymeric mixed conductors, $p(C_6NDI-T)$, P-90, and P-75, were based on chloroform, while BBL and gAIID-2FT were prepared in methanesulfonic acid (MSA) solution and $60:1$ chloroform : chlorobenzene solution, respectively. We used 5 mg ml$^{-1}$ concentration for all polymers.

p($C_6$NDI-T) and P-90 films were spin-coated at 650 rpm for 45 s. gAIID-2FT and P-75 films were spin-coated at 1000 rpm and 800 rpm for 60 s, respectively. BBL solution and the substrate were heated before coating at 90 °C and 65 °C, respectively. BBL films were spin-coated at 1000 rpm for 60 s. To remove MSA from films, the BBL-coated surfaces were immersed in water for 30 minutes. All BBL films were soft-baked at 110 °C for 1 min, and the sacrificial top layer of parylene C was peeled off to pattern the channel and gate coatings. BBL based OECTs were then annealed at 110 °C for 1 hour.

### Spectroelectrochemistry

Ocean Optics HL-2000-FHSA halogen light source, QP600-1-SR-BX optical fibers, and Ocean Optics QE65 Pro Spectrometer were used to measure the UV-Vis spectra of the polymers. An ITO substrate placed in PBS inside the sample holder (MM SPECTRO-EFC) was used as a blank for calibration. Polymer films were spin-coated on ITO substrates as described above. A potentiostat (PalmSens, PalmSens4) was connected to ITO, Ag/AgCl reference electrode, and platinum (Pt) counter electrode, where all were immersed in the electrolyte. The polymers were electrochemically cycled from 0.2 V to −0.7 V with respect to Ag/AgCl reference electrode at 0.1 V step. OceanView software was used to record the spectra.

### Light source and calibration

For the light condition of this study, a deep red LED (655 nm) from Autolab Optical bench (Metrohm AG, Herisau, Switzerland) was used. The light intensities of the light source were calibrated by using PM100D light power meter working with an S130VC photodiode power sensor (Thorlabs, Inc., Newton, NJ, USA). The distance between the films or the photodiode power sensor used during the calibration was set at 3 cm from the light source.

### Electrochemistry measurements

A three-electrode setup was used for electrochemical measurements of the polymer-coated Au electrode addressed as a working electrode (500 × 500 μm$^2$) with Ag/AgCl as the reference electrode and Pt wire as the counter electrode. All measurements were performed in PBS under dark and light conditions in ambient or $N_2$ atmospheres using VSP 300 BioLogic Science Instrument potentiostat. Cyclic voltammograms were collected by sweeping the potential at the working electrode from 0.2 to −0.8 V *versus* the Ag/AgCl reference electrode at a 50 mV s$^{-1}$ scan rate. Open circuit potential (OCP) of the films was recorded after leaving the film surface covered in PBS overnight, which stabilized the values. The electrochemical impedance spectra of these electrodes were measured in a frequency range of 10 kHz to 1 Hz with 10 mV modulation amplitude and at 0 V *versus* OCP. LUMO levels were estimated using the onset of reduction potentials observed in cyclic voltammograms. The curves were obtained in $N_2$-degassed electrolyte (acetonitrile, 0.1 M TBA-NPF6) in the absence of $O_2$ to eliminate any contribution from oxygen reduction reactions. The curves were identical for consecutive measurements. The ferrocene/ferrocenium (Fc/Fc$^+$) redox couple was used as a reference, and all potentials were converted, assuming 4.8 V as the ionization energy of Fc/Fc$^+$.

### OECT and OPECT characterization

Dual-channel Keithley 2602A source-meter (Tektronix, Inc., Beaverton, OR, USA) operated by a customized LabVIEW software was used for OECT characterization. All measurements were performed in ambient conditions using PBS as the electrolyte. The current–voltage characteristics were recorded in dark and light conditions. The OECT currents in dark and light conditions were monitored in real time at a constant gate voltage and constant source–drain voltage. The deep red light was used after obtaining a steady baseline of the channel current. The devices were switched on and off with gate voltage or light pulses and current was monitored over time. Switching on or off time of the devices ($\tau$) was estimated by fitting the rising curve with an exponential decay function. For light-induced switching time, we reported the rise time, that is, the time it required for $I_D$ to go from 10% to 90% of its maximum level. The fall time corresponds to the period after light was switched off, was calculated as $I_D$ going from 90% to 10% of its stable level. The responsivity, detectivity, and sensitivity of OPECTs were calculated using $R = \dfrac{I_{light} - I_{dark}}{P_{light}}$, $D = \dfrac{R}{\mathrm{sqrt}(2 \times q \times I_{dark})}$, $S = \dfrac{I_{light}}{I_{dark}}$, respectively. The $I_{light}$ is the current recorded in light conditions, $I_{dark}$ is the current obtained in dark conditions, $P_{light}$ is light power density, and $q$ represents electron charge.

### Transient absorption (TA) spectroscopy

TA spectroscopy was carried out using a home-built pump–probe setup. The output of a Ti:sapphire amplifier (Coherent LEGEND DUO, 800 nm, 4.5 mJ, 3 kHz, 100 fs) was split into four beams (2 mJ, 1 mJ, 1 mJ, and 0.5 mJ). Three of them were used to separately pump three optical parametric amplifiers (OPA; Light Conversion TOPAS Prime). One of the 1 mJ TOPAS generates wavelength-tunable pump pulses (240–2600 nm, using Light Conversion NIRUVIS extension), which was fixed at 660 nm. A fraction of the 0.5 mJ output of the Ti:sapphire amplifier was focused into a c-cut 3 mm thick sapphire window, thereby generating a white light supercontinuum from 500 to 1800 nm. The pump–probe delay time was achieved by varying the probe path length using a broadband retroreflector mounted on a 600 mm automated mechanical delay stage (Newport linear stage IMS600CCHA controlled by a Newport XPS motion controller), generating delays from −400 ps to 7 ns.

Pump and probe beams were focused on the sample to spot sizes of 1.0 mm and 0.10 mm diameter (from a Gaussian fit at 86.5% intensity), as measured using a beam profiler (Coherent LaserCam-HR II). The samples were kept under a dynamic vacuum of $< 10^{-5}$ mbar, and pump and probe beams were incident on the substrate side of the sample (*i.e.*, closer to the ITO/polymer interface). The transmitted fraction of the white light was guided to a custom-made prism spectrograph (Entwicklungsbüro Stresing) where it was dispersed by a prism onto a 512-pixel CMOS linear image sensor (Hamamatsu G11608-512A). The probe pulse repetition rate was 3 kHz, while

the excitation pulses were mechanically chopped to 1.5 kHz, while the detector array was read out at 3 kHz. Adjacent diode readings corresponding to the transmission of the sample after excitation and in the absence of an excitation pulse were used to calculate $\Delta T/T$. Measurements were averaged over several thousand shots to obtain a good signal-to-noise ratio. The chirp induced by the transmissive optics was corrected with a home-built Matlab code.

### Doping-induced absorption spectroscopy (DIA)

Molecular doping was used to generate negative charges using a strong one-electron dopant Cobaltocene. Polymer films were spin coated on a pre-cleaned quartz substrate as described above; subsequently, the dopant was spin-coated on the top at 2000 rpm for 45 s. Cobaltocene was dissolved in an orthogonal solvent, isopropanol (IPA), with a concentration of (0.3 mg ml$^{-1}$) to create a bilayer without dissolving the polymer films underneath.

To characterize the doped film, UV-Vis absorption spectra of the film were measured before and after doping. Upon doping, the absorbance of the polymer film changes; and this change can be calculated using the differential transmission formula as follows:

$$\frac{\Delta T}{T} = 10^{-\Delta A} - 1 = \left(\frac{T_{\text{doped}} - T_{\text{neat}}}{T_{\text{neat}}}\right)$$

where $T_{\text{neat}}$ and $T_{\text{doped}}$ are the transmittances of the neat and doped film and the resulting spectrum is assigned to anion.

### Time-resolved THz spectroscopy (TRTS)

TRTS was carried out using a home-built setup, using the same Ti:sapphire amplifier as for the TA spectroscopy. A second TOPAS (2 mJ) generates wavelength-tunable pump pulses (240–2600 nm, using Light Conversion NIRUVIS extension), which was fixed at 500 nm. A fraction of the 0.5 mJ fundamental output of the Ti:sapphire amplifier was split into 2 additional beams: one used for THz generation, and the other for THz gating. The THz emitter and detector were two 1 mm thick ⟨110⟩ oriented zinc telluride (ZnTe) crystals. All the THz-related optics were placed in a closed chamber, continuously purged with pure N$_2$ gas. THz probe pulses and optical pump pulses were chopped at 499 Hz and 3 × 499 Hz by two optical choppers, respectively, to collect dark and excited state signals with one lock-in amplifier by adjusting its harmonic reference.

## Results and discussion

### Electrochemical response of n-type films to light

The chemical structures of the n-type polymers, p(C$_6$NDI-T), P[(NDI2OD-T2)0.1-ran-(g7NDI-T2)0.9] (P-90), poly(benzimidazobenzophenanthroline) (BBL), gAIID-2FT, and P-75, are shown in Fig. 1(a). Some of these polymers have previously been shown to operate in an OECT channel gated with Ag/AgCl electrode through an aqueous electrolyte such as sodium chloride (NaCl). We chose these polymers to evaluate their performance in OPECTs as they have distinct chemical structures and are representatives of the current library of n-type

OECT materials. Except for BBL, all have polar ethylene glycol (EG) units attached to their backbone, allowing ion uptake and transport through their bulk. P-90, p(C$_6$NDI-T), and gAIID-2FT have a donor–acceptor type backbone. P-90 is a random copolymer made of the widely studied naphthalene diimide (NDI) acceptor combined with a bithiophene donor.[20] Its structure contains 90% of the glycolated NDI-T2 monomer and 10% of the same monomer where EG chains are replaced with alkyl chains. p(C$_6$NDI-T) differs from P-90 with its single thiophene donor unit and the conjugation of the EG side chains through a 6-carbon spacer. The other donor–acceptor polymer is gAIID-2FT, based on a diazaisoindigo acceptor and a fluorinated thiophene donor.[21] The remaining polymers (P-75 and BBL) have only acceptor units. P-75 is a lactone-based rigid copolymer bearing benzene and naphthalene building blocks with a large electron affinity.[23] The high benzene content in the core reduces the backbone twisting, leading to high electron mobility, and this polymer has not been examined before as an OECT channel material. BBL has, similarly, a planarized, rigid backbone but no side chains.[24] These polymers have LUMO values within the range of 4.2 to 4.9 eV, with gADII-2FT having the lowest and P-75 having the highest value (see Fig. S1, ESI† for cyclic voltammetry (CV) curves used for electron affinity determination and Table S1, ESI† for the values).

We coated thin polymer films on indium tin oxide (ITO) substrates to collect their UV-Vis-NIR spectra. All films were immersed in phosphate-buffered saline solution (PBS, 0.1 M) and electrochemically doped/dedoped with respect to Ag/AgCl electrode. Fig. 1(b) shows the spectrum of each polymer film at open circuit potential (OCP). All polymers exhibit a strong ground state absorption in the visible region (440 nm to 750 nm). In addition to the absorption in the visible, P-75 also shows a higher wavelength feature, that is attributed to polarons.[22] Fig. S2 (ESI†) shows the spectral evolution of each film addressed with increasing voltages towards more negative values vs. Ag/AgCl. At higher negative voltages, we observe the bleaching of these ground state absorption features and the generation of new lower or higher energy bands, attributed to polaronic or multi-polaronic species, in line with previous studies.[21,23–25] For P-75, we observe that the negative voltages applied to the film decrease the intensity of all spectral the features covered by our detector (until 1100 nm). These results confirm that the optical transitions of the films can be electrochemically modulated in an aqueous electrolyte. For all films, except P-75, the electrons injected from the ITO are stabilized by the PBS cations penetrating the films, changing the bandgap.

Having confirmed the absorption of the films in the visible region and their electrochemical response, we performed a series of electrochemistry experiments in a standard three-electrode configuration in the dark and upon illumination with a light-emitting diode (LED) at a peak wavelength of 655 nm (a region where all polymers absorb at a similar strength), as illustrated in Fig. 1(c). Cyclic voltammograms of all polymer films before and during light illumination are shown in Fig. 1(d). The intrinsic (dark) CV curves of p(C$_6$NDI-T) and P-90 are alike, exhibiting three distinct redox peaks between
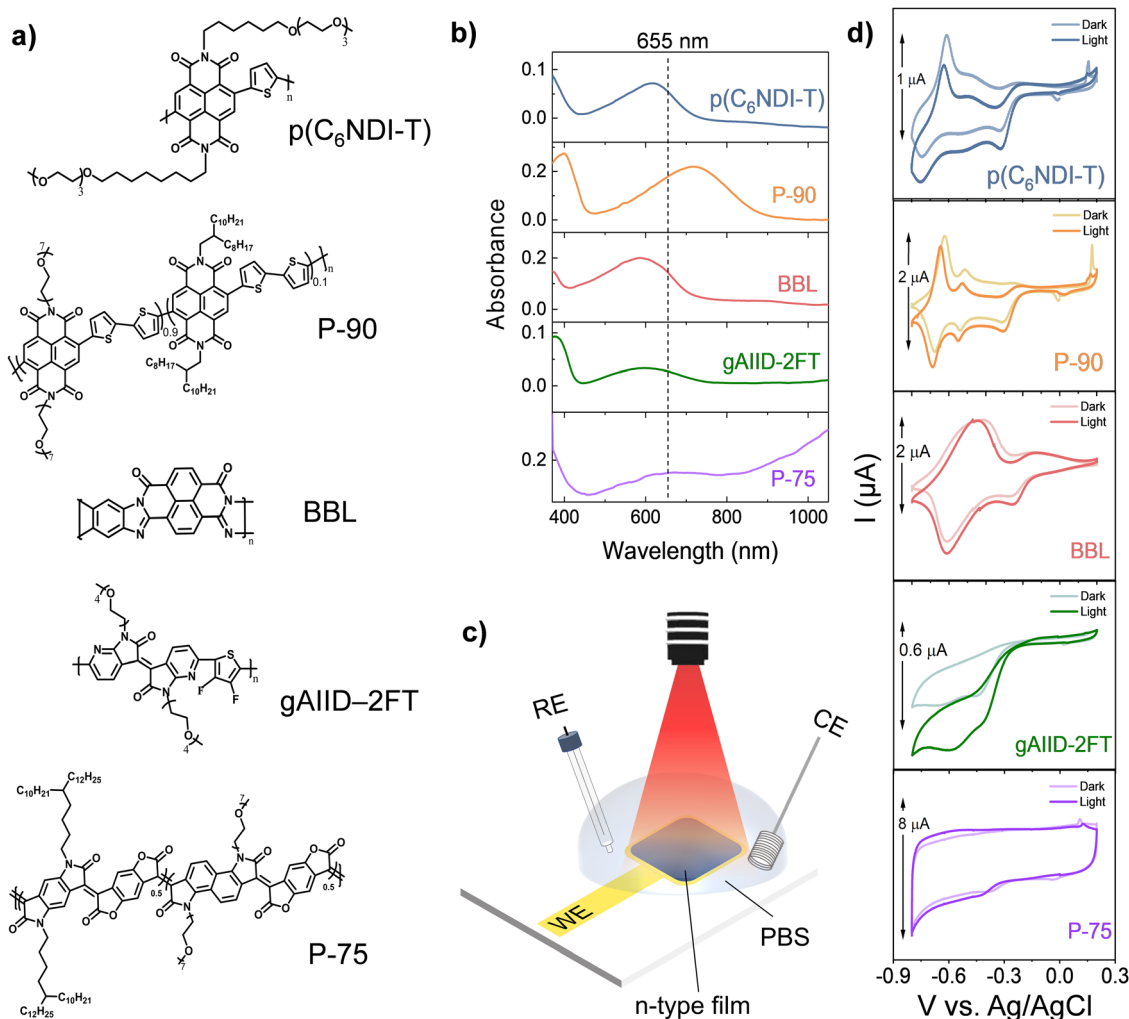
**Fig. 1** (a) The chemical structures of the n-type polymeric mixed conductors: p(C$_6$NDI-T), P-90, BBL, gAIID-2FT, and P-75. (b) The absorption spectra of the n-type films in an aqueous PBS solution (0.1 M). The films were at OCP conditions. (c) The three-electrode configuration used for the electrochemical characterization of the films (working electrode, WE) coated on an Au electrode (500 × 500 μm$^2$) covered with a drop of PBS into which the reference electrode (RE) and the counter electrode (CE) were immersed. Not to scale. (d) CV curves of the films recorded in the dark and under red light illumination (655 nm, 0.258 W cm$^{-2}$). The scan rate was 50 mV s$^{-1}$. The forward cycle starts from the positive range and extends till −0.8 V vs. Ag/AgCl.

−0.25 V and −0.8 V vs. Ag/AgCl attributed to oxygen reduction reaction (ORR), polaronic and bi-polaronic species formation.[28] For BBL, we observe two peaks, one at a lower reductive potential (−0.3 V) attributed to ORR, and another around −0.6 V vs. Ag/AgCl.[25,26] For gAIID-2FT, no oxidation peaks exist but there is a sharp reduction peak at similar potentials to others. P-75 displays a very different behavior; it has a box-like (capacitive) cyclic voltammogram and reduction currents with much larger amplitude. Upon light illumination, for all films, no redox peaks are lost, or new ones appear. There are also no significant changes in the peak positions. The only noticeable change in all voltammograms, except for P-75, is a downward shift of both anodic and cathodic currents. This change in a CV curve is reminiscent of the effect of oxygen (O$_2$) on the CV curve of an n-type film.[24,25] We observe that, for the n-type films, O$_2$ causes an increase in the reduction currents and the appearance of a shoulder at low negative potentials (around −0.2 V) (Fig. S3, ESI†). These observations lead us to conclude that

illuminated n-type films exhibit larger ORR currents. The larger currents observed in the light conditions suggest that light enhances the capability of the films for ORR but does not generate new redox states. Here, gAIID-2FT film exhibits the most significant change in the peak current values upon light exposure, while P-75 voltammogram is insensitive to illumination conditions.

Next, we monitored the open circuit potential (OCP) of the films in PBS vs. Ag/AgCl reference electrode as they were illuminated. Fig. 2(a) demonstrates that the OCP shifts toward more negative values upon exposure to light. Once the light is switched off, the electrochemical potential reverts to its initial value in the dark. The light-triggered change in OCP is repeatable, meaning that OCP goes up and down depending on the presence of light and is reversible as long as the OCP stabilizes within the monitored time. The OCP changes more rapidly with excitation (light on) than relaxation (light off). The excitation of polymers seems to be similarly long for all films, but the
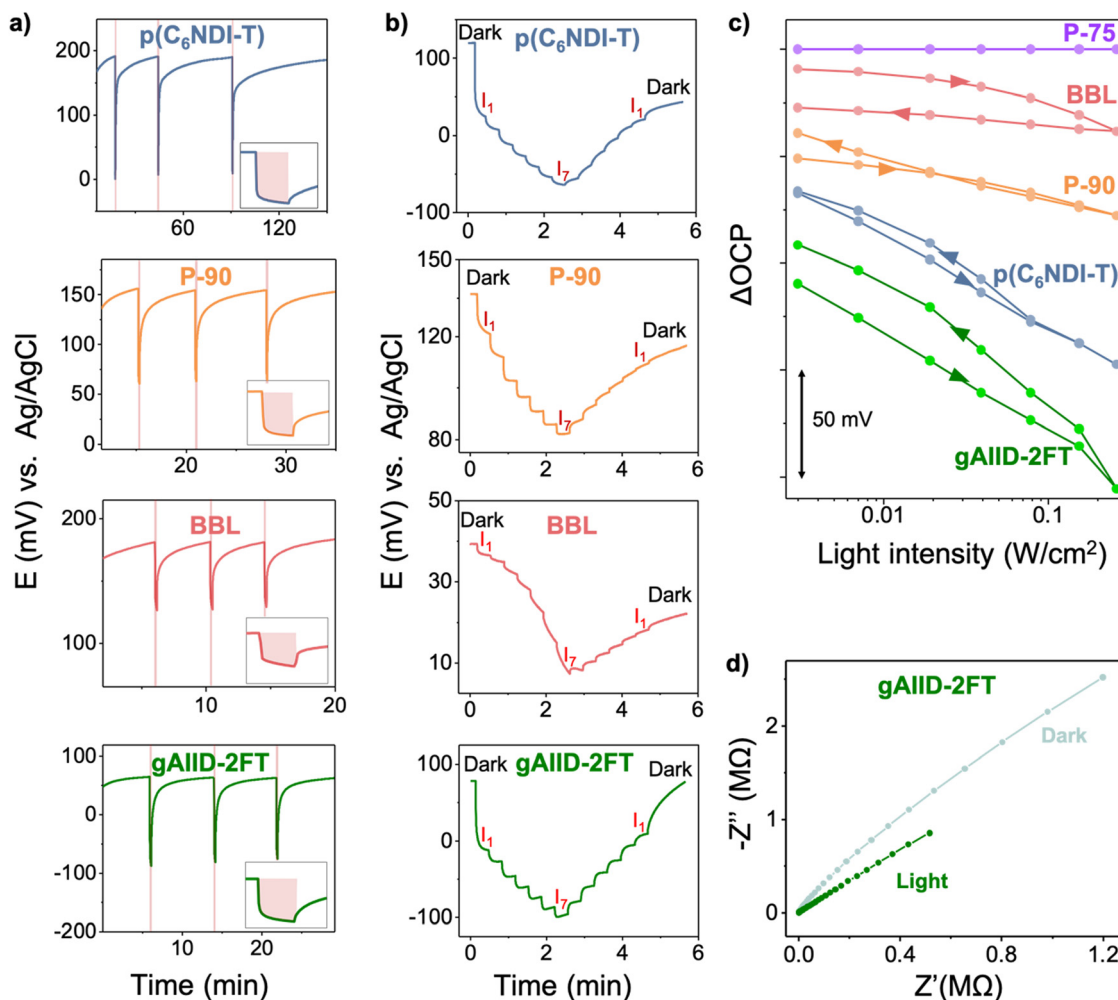
**Fig. 2** (a) The OCP of p($C_6$NDI-T), P-90, BBL, and gAIID-2FT films monitored in PBS, first in the dark and upon three consecutive light pulses (10 seconds ON and OFF until the OCP recovery). The LED power was 0.258 W cm$^{-2}$. The shaded areas represent the light exposure period. (b) The real-time change in OCP as a function of light intensity, first increasing from 0.003 to 0.258 W cm$^{-2}$ ($I_1$ to $I_7$) and then ramped down to the initial light intensity ($I_7$ to $I_1$). The corresponding intensity values of $I_1$, $I_2$, $I_3$, $I_4$, $I_5$, $I_6$ and $I_7$ are given in Table S2 (ESI†). (c) The absolute change in OCP values (OCP$_{dark}$ − OCP$_{light}$) at different light intensities. The arrow shows the direction of the light-intensity scan. (d) Nyquist plots of gAIID-2FT at 0 V *vs.* OCP in the dark and light conditions.

relaxation times are different, with p($C_6$NDI-T) taking longer to reinstate its dark potential, followed by gAIID-2FT, P-90, and BBL (see insets to Fig. 2(a)). Notably, the OCP of P-75 is insensitive to light despite its strong absorption at this wavelength (Fig. S4a, ESI†).

To investigate a potential correlation between OCP and light intensity, after recording the electrochemical potential in dark conditions, we increased the illumination intensity of the LED gradually from 0.003 to 0.258 W cm$^{-2}$ and then ramped it back down to dark conditions, as shown in Fig. 2(b). We observed a gradual decrease in OCP for all polymers (except for P-75) with an increase in light intensity. During the ramp-down of the light intensity, some polymers quickly relaxed back to their original values, while others took longer. Fig. 2(c) depicts that gAIID-2FT film has the highest change in OCP for all light intensities, followed by p($C_6$NDI-T), P-90, and BBL. From dark to 0.258 W cm$^{-2}$ illumination, the OCP of gAIID-2FT changed by 200 mV *vs.* Ag/AgCl, whereas for p($C_6$NDI-T), P-90, and BBL,

this value was 180, 60, and 20 mV, respectively. Note that illuminating the electrode from different sides of the device (*i.e.*, the polymer side as depicted in Fig. 1(c) or the ITO side) leads to different absolute changes in OCP as well as its dynamics. For example, for p($C_6$NDI-T), there is a higher change and a faster drop in OCP when the light hits the polymer side (Fig. S4b, ESI†). To be consistent across the experiments and alleviate the reliance on transparent substrates like ITO for device fabrication, we chose to work with the polymer-side illumination configuration.

Light also increases the current collected at OCP conditions, except for P-75, as shown in Fig. S4c (ESI†). The current reaches a stable value after the initial capacitance-based spike and maintains this value during light pulse period. Light reduces the total impedance (absolute value of modulation) at the same frequency, as demonstrated by the Nyquist plots recorded under dark as well as light conditions (see Fig. 2(d) for p($C_6$NDI-T), and Fig. S5 (ESI†) for other polymers). Note that

since most films are semiconducting at OCP conditions and the spectra are dominated by ion diffusion inside the films, the equivalent circuit modeling is not straightforward. Overall, we conclude that light induces a drop in the OCP of the films while reducing their electrochemical impedance and increasing ORR currents. The gAIID-2FT and p($C_6$NDI-T) films show a larger photoelectrochemical response than other polymers, while P-75 has no change in its electrochemical characteristics upon light exposure. Note that the extent of the photoresponse is not correlated with electron affinities, hence the ease of electron injection from the contacts does not govern the photoelectrochemical performance. We thus sought to understand the differences in photoelectrochemical characteristics using ultra-fast spectroscopy.

### Photophysical properties of n-type mixed conductors

Transient absorption (TA) spectroscopy is sensitive to small changes in transmission upon photoexcitation ($\Delta T/T$), and evaluation of the spectro-dynamics can help differentiate between different photo-excited species. We recently reported the TA spectra of p($C_6$NDI-T) and demonstrated that the excited state of this polymer consists of three dominant species: (1) pronounced photoinduced absorption (PA) of excitons (PA$_{ex}$; 900–1100 nm); (2) PA from charges, particularly at higher excitation densities (PA$_{ch}$; 690–850 nm); and (3) and PA from intra-molecular charge transfer (ICT) excitons (PA$_{ict}$; 1250–1500 nm),

particularly in the presence of ITO (reproduced in Fig. 3(a) and Fig. S6, ESI†).[18] We identified the three species by comparing the intrinsic p($C_6$NDI-T) spectra to the p($C_6$NDI-T)/ITO spectra and the doping-induced absorption (DIA, or in this case, anion) spectra.

We evaluated the other four polymers using the same three spectra (intrinsic n-type polymer film; polymer/ITO; and anion spectra) and found marked differences in the species present (Fig. S7–S11, ESI†). P-90 showed the most similar behavior to p($C_6$NDI-T), exhibiting PA from charges, excitons, and ICT states at 850–940 nm, 1020–1150 nm, and 1300–1500 nm, respectively (Fig. 3(a) and Fig. S7, ESI†). BBL and gAIID-2FT did not exhibit PA from ICT states within the spectral range of our experimental setup but exhibited PA of charges and excitons (Fig. 3(a) and Fig. S8, S9, ESI†). Finally, P-75 demonstrated no observable PA from either excitons or ICT states within the spectral range of our setup, and the presence of ITO had almost no impact on the excited state spectra (Fig. 3(b) and Fig. S10, ESI†). The PA$_{ch}$ from P-75 was markedly more pronounced than from any of the other polymers, whereas the PA$_{ex}$ from gAIID-2FT was the most pronounced. Recall that P-75 showed no response to light whereas gAIID-2FT had the highest OCP change. These results indicate that the presence of excitons, rather than charges, is crucial for the photoelectrochemical response of a material.

To quantify the dependence of the photosensitivity on the material type, we compared the pump–probe kinetics of the



**Fig. 3** TA spectroscopy of films on bare glass or on ITO/glass. (a) TA spectra of intrinsic films (light lines) and polymer/ITO films (dark lines), averaged over pump–probe delay times of 0–1 ps. The pump wavelength was 660 nm for all samples, and the irradiance was 36 mW cm$^{-2}$ for p($C_6$NDI-T); 26.7 mW cm$^{-2}$ P-90, BBL, and gAIID-2FT and 73.9 mW cm$^{-2}$ for P-75. Overlaid are the doping-induced absorption (DIA) anion spectra (light dashed line), for all films except BBL. (b) Picosecond-nanosecond kinetics of the polymer/ITO films, averaged over their dominant photoinduced absorption (PA) signals (*i.e.*, 950–1050 nm for p($C_6$NDI-T); 1020–1150 nm for P-90; 1030–1230 nm for BBL; 1050–1350 nm for gAIID-2FT; and 1300–1550 nm for P-75). Overlaid are the multi-exponential decay fits. (c) Amplitude-averaged lifetimes of decaycomponents calculated from the multi-exponential fits (see Table S3, ESI†).

dominant PA signals (Fig. 3(b)). In all cases except for P-75, the dominant signal was PA$_{ex}$; for P-75, there were two PA$_{ch}$ species, and the dominant signal was for the lower energy one (*i.e.*, PA$_{ch}$, 2). There was a very pronounced difference in the lifetime of the different PA species for all materials, with gAIID-2FT having the longest PA$_{ex}$ lifetime, and P-75 having almost no $\Delta T/T$ signal after only 1 ps. Such ultrafast excited state relaxation is indicative of self-doping of the polymer, leading to intrinsic conductivity in the dry film, and fast relaxation by exciton–polaron annihilation.[27,28] This was further confirmed by THz spectroscopy measurements, which showed the P-75 had a ground state conductivity of 190.8 $\Omega$ cm$^{-1}$ (Fig. S12,

ESI†). By fitting the kinetics with multi-exponential decays, we extracted the amplitude-averaged lifetimes of the dominant PA signals as shown in Fig. 3(c) and summarized in Table S3 (ESI†). The lifetime of the dominant PA signals correlated directly with the increase in photovoltage, with gAIID-2FT having the longest lifetime, followed by p(C$_6$NDI-T), P-90, BBL, and P-75. The rapid relaxation of the PA signal from P-75 explains why the material has almost no change in OCP upon illumination: there is insufficient time for photoexcited carriers to contribute to voltage build-up. From these results, we can conclude that longer PA lifetimes should lead to greater changes in OCP, hence materials that have long-living excitonic
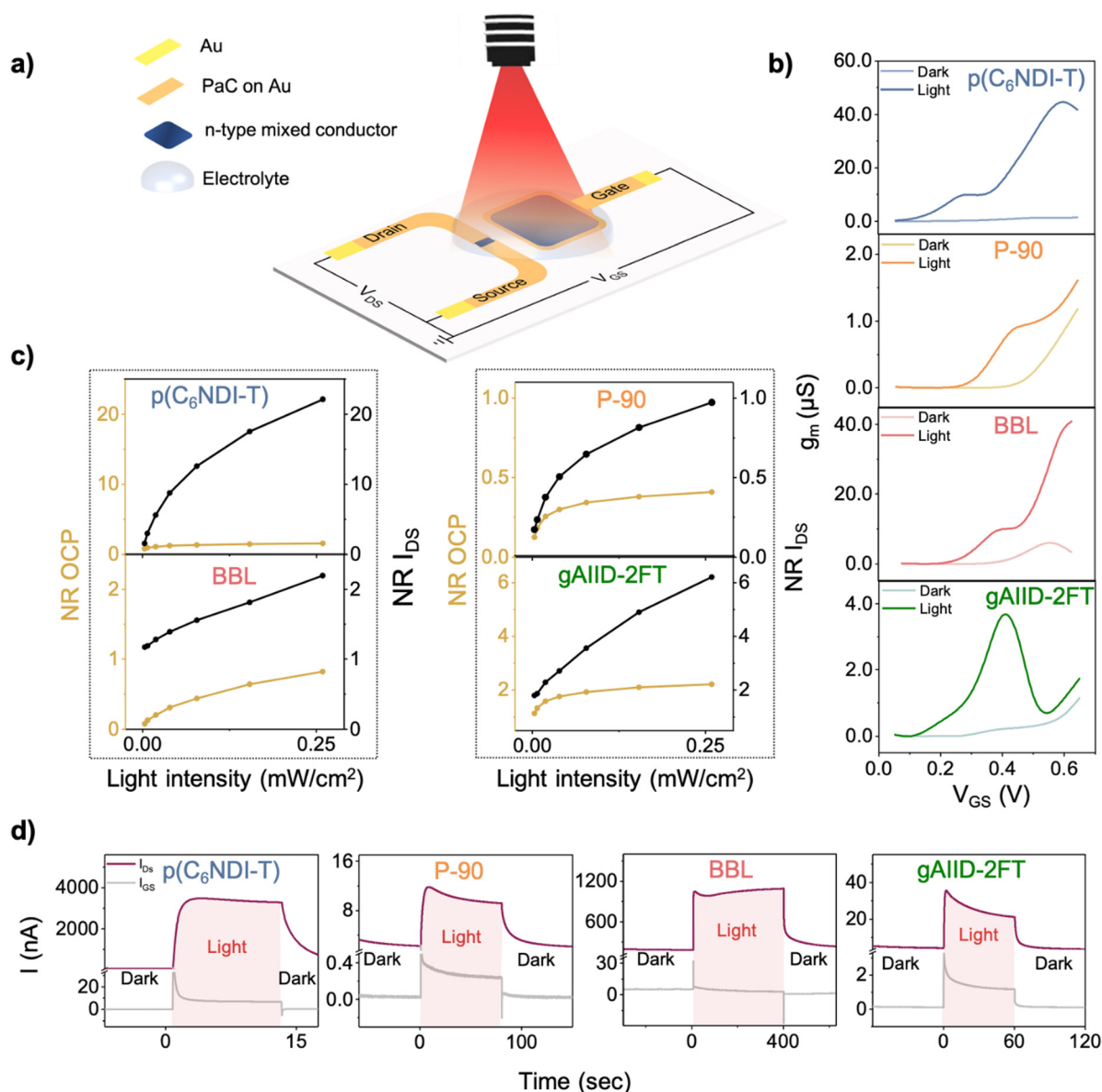


Fig. 4 (a) Schematic of the n-type OPECT. Not to scale. (b) Transconductance ($g_m$) versus gate voltage ($V_{GS}$) of the OPECTs in dark and light conditions. $V_{DS}$ = 0.4 V. (c) The comparison of each device performance for detecting light intensity variations. The normalized response of the electrode and the OECT is calculated as the light-induced change in electrochemical potential ((OCP$_{Light}$ − OCP$_{Dark}$)/OCP$_{Dark}$), and in channel current (($I_{DS(Light)}$ − $I_{DS(Dark)}$)/$I_{DS(Dark)}$), respectively. (d) The real-time change in $I_{GS}$ and $I_{DS}$ upon light illumination at 0.258 W cm$^{-2}$. The shaded area represents the light exposure period. $V_{GS}$ = $V_{DS}$ = 0.4 V. The film thickness is 240 nm for p(C$_6$NDI-T), 150 nm for P-90, 120 nm for BBL and 400 nm for gAIID-2FT.

states are most promising for high photoelectrochemical response.

### Evaluating n-type OPECT characteristics

After confirming and comparing the photosensitivity of n-type mixed conductors, we fabricated micron-scale OECTs with the film patterned in the channel ($100 \times 10 \ \mu m^2$) and as a coating on an Au electrode ($0.25 \ mm^2$) adjacent to the channel on the same chip. Fig. 4(a) provides a schematic representation of the OPECT configuration and operation, where a light source is positioned on top of the gate electrode. To assess the performance of these OECTs, we examined the transfer curves (Fig. S13a, ESI†), showing that the channel currents of all OECTs bearing the photosensitive films increased upon illumination. The current increase from dark to light conditions was found to be 36-fold for p($C_6$NDI-T), 6.5-fold for BBL, 5.8-fold for gAIID-2FT, and 2.5-fold for P-90 (reported at $V_{GS} = V_{DS} = 0.4$ V). OPECTs exhibited earlier threshold voltages under illumination, implying that lower voltages are required to dope the channel in the presence of light (Fig. S13b, ESI†). The $g_m$ of the transistors increased dramatically upon illumination, 23.6-, 20.6-, 16.3-, and 3.8-fold for p($C_6$NDI-T), P-90, gAIID-2FT, and BBL, respectively (Fig. 4(b)). Light, when used in combination with voltage, enhances the gating efficiency, leading to $g_m$ values, which are otherwise theoretically not possible within the operation range of these transistors. This is an appealing approach to increase the amplification without having to modify the device geometry, operation conditions, or materials used. Note that characteristics of P-75 OECTs remained unchanged under illumination (Fig. S14, ESI†).

We also examined the photoresponse of the device configuration, which integrates a non-photoresponsive gate electrode (Ag/AgCl pellet) with the same polymeric channels. Fig. S13c (ESI†) shows that there is an increase in the channel current with light illumination; however, the change is not as substantial (1.2-fold for p($C_6$NDI-T), P-90, and BBL and 1.02-fold for gAIID-2FT at a maximum gate voltage of 0.6 V) as when the n-type film is used as the photosensitive gate electrode. This result is unsurprising since OECTs transduce and amplify voltage changes at the gate electrode. Therefore, using the investigated polymers as the single functional material in OPECTs not only simplified the device design but also enhanced the photosensitivity.

The impact of light on OECT steady-state characteristics is consistent with the light-induced shift in the film's electrochemical potential observed in Fig. 2(a) and (b). Upon illumination, two mechanisms contribute to the increase in OECT channel currents and gain: (1) the shift of gate OCP and (2) the decrease in gate impedance. When the photosensitive n-type material at the gate electrode is electrochemically reduced by light, resulting in a lower impedance gate material, the channel is driven to a more reduced state that can be achieved at lower voltages. Consequently, we observe an increase in channel current at the same biasing conditions and improved gains when light is present during device operation. The high photosensitivity of p($C_6$NDI-T) and gAIID-2FT – large OCP and

impedance changes with light – enable their OECTs to achieve the greatest transduction enhancement upon illumination. The advantages of employing these materials in an OECT configuration are numerous. In Fig. 4(c), we compare the light detection performance of the n-type films in the electrode and the OECT configuration and evaluate which device type yields a larger photovoltage or photocurrent response. Using the transistor allows for a higher change in the device output (i.e., the normalized response). The OECT also shows a lower limit of detection and higher sensitivity to various light intensities, highlighting the importance of the amplification feature inherent to the OECT configuration. The gate electrode can be paired with different channel materials, which may allow for even higher sensitivities.

The amplification of the OECT is also evident when we compare the light-induced changes in the gate current ($I_{GS}$) with those in the channel current. Typically, the dark $I_{GS}$ is 193, 163, 42, and 15 times lower than the $I_{DS}$ of BBL, p($C_6$NDI-T), P-90, and gAIID-2FT OECTs, respectively (Fig. 4(d)). The disparity between channel and gate currents becomes more pronounced under light exposure. Fig. 4(d) shows that both the gate and channel currents change promptly with light; however, the change in $I_{DS}$ is dramatically higher due to OECT amplification. In illuminated conditions, the $I_{DS}$ is 427, 243, 49, and 20 times larger than $I_{GS}$, for p($C_6$NDI-T), BBL, P-90, and gAIID-2FT, respectively. Note that the additional $I_{GS}$ observed under light is not a photocurrent but originates to compensate for the light-enhanced ORR of the channel. This conclusion is supported by the observation that even though the channel current increased with light in an $O_2$-depleted environment, $I_{GS}$ did not change (Fig. S15, ESI†). These results prove that the n-type OPECT developed in this work does not rely on faradaic events, and its operation is driven by potentiometric changes at the gate electrode.

Fig. 4(d) illustrates some differences between the ON and OFF switching speeds of these phototransistors. Recall also that we noted variations, particularly in the recovery behavior of the OCP after the light was switched OFF (Fig. 2(a)), with prolonged times as the OCP change increases. To investigate the factors determining device response time to a light pulse, we first characterized the speed of current change in response to a voltage pulse. Switching on (or off) times ($\tau$) were estimated by using an exponential fit and summarized in Table S4 (ESI†). With an Ag/AgCl gate, all OECTs turned ON within a few milliseconds, with small differences that can be explained by varying film thicknesses (Fig. S16, ESI†). However, with polymer gates, the differences became more pronounced, with all devices operating much more slowly (Fig. S17, ESI†). Notably, the gAIID-2FT exhibited the fastest speed (18 ms), whereas BBL was the slowest (220 ms). These differences appear to be related to differences in the capacitance of these films. BBL has a much larger volumetric capacitance ($C^* = 731$ F cm$^{-3}$) compared to the other films ($C^* = ca.$ 260 F cm$^{-3}$ for P-90 and p($C_6$NDI-T), while gAIID-2FT has the smallest $C^*$ of 95 F cm$^{-3}$). When polymers gate the channel, their ability to accept counterions into their bulk slows down device operation.

Next, we extracted the time it took for the current to reach 90% of its final value under illumination and the rate at which it returned to 10% of the final dark value using a set of controlled real-time experiments shown in Fig. S18–S21 (ESI†). We observed a consistent trend in the rise and fall response times, with the recovery being slower than the current buildup, similar to the OCP dynamics (Table S5, ESI†). The speed of current drop once the light is switched off follows exactly the inherent speeds of the devices. For instance, the slowest OECT (BBL-based) also exhibits the slowest fall time. The fastest device, gAIID-2FT, generates the fastest recovery. However, the rise time of gAIID-2FT device is slower than its fall time. We attribute this difference to the very high sensitivity of gAIID-2FT to light (*i.e.*, the largest change in OCP). Similarly, the film that is the least responsive to light (*i.e.*, the smallest change in OCP) very rapidly generates a current build-up upon illumination. Overall, we hypothesize that a combination of initial speeds (governed by the $C^*$ of the polymeric gates) and the extent of light sensitivity determines the switching ON time of the current in response to a light pulse. Fig. S18–S21 (ESI†) also illustrate the impact of varying light pulse durations on channel current–time profiles. While the maximum current values do not change, the device currents do not reach a stable value until

10 s and with longer pulses (above 30 s), the current experiences a decline.

We observe a reduction in current after reaching a maximum for a single 1-minute-long pulse (see Fig. S18–S21, ESI†), but it remains unclear if the same photocurrents can be regenerated with subsequent pulses. We operated the devices with 1-minute long on and off light pulses continuously over 3 hours and monitored the channel current. Fig. 5 (left) shows a very high initial current build-up during the light pulse, followed by a decrease over time. Among all polymers, p($C_6$NDI-T) exhibited the highest current retention, with 55% of the initial current maintained at the end of light on–off cycles. To investigate whether the decrease in current over time is caused by light exposure, we examined the current behavior in the dark under the same biasing conditions. The p($C_6$NDI-T) and P-90 devices experienced a loss of output current, particularly during the initial hour of operation before stabilization, as shown in Fig. 5 (middle). Similar behavior was observed for gAIID-2FT, where the current decreased significantly at the start of biasing but achieved a stable readout thereafter. BBL exhibited a continuous decrease in current over time under constant biasing conditions. This analysis revealed that the decrease in current over time is an inherent characteristic of the device,



**Fig. 5** The stability of OPECTs. Left: The channel current of the OPECT monitored over three hours ($V_{DS} = V_{GS} = 0.4$ V) under light pulses (ON for 1 min, OFF for 10 min) middle: in the dark. The polymer gates were used. Right: The channel current of the OPECT monitored over three hours in the dark ($V_{DS} = V_{GS} = 0.4$ V), where Ag/AgCl was used as a gate and p($C_6$NDI-T), P-90, BBL and gAIID-2FT used as a channel of OECTs.

indicating that there is no adverse effect of light on films' electronic properties. This result is surprising as these channel materials have been shown to be very stable in previous studies.[18,21,22,26] When Ag/AgCl is used as a gate electrode, the polymer films in the channels are fairly stable against long-term operation (Fig. 5 (right)). These results suggest that the current drop observed in Fig. 5 (left and middle) arises from the polarization of the polymer-coated gated electrode rather than any degradation of the material itself. Light-induced polarization can become a feature for the development of neuromorphic devices since polarization can be controlled by light pulse intensity, duration, and frequency.[13,29] On the other hand, it is worth noting that the experimental conditions used for the above continuous operation tests are extreme, as the devices are subjected to prolonged operation without rest. For biosensing applications, the effect of light pulse length and operation duration should be considered and included in the device design.

### OPECT performance as a photodetector

We next conducted experiments to assess the response of each OPECT while varying the light intensity under continuous biasing. Fig. 6(a) illustrates that $I_{DS}$ follows the change in the light intensity, *i.e.*, it increases (decreases) with an increase (decrease) in light power. Remarkably, even the lowest intensity provided by our light source (0.003 W cm$^{-2}$) elicited a response from the devices thanks to the photosensitivity of the polymers combined with the high $g_m$ of the OECTs. In Fig. 4(c), we highlighted the higher light sensitivity of the OPECT compared to the electrode configuration. Here, we note another advantage

of the OECT, *i.e.*, its faster response to light and enhanced reversibility. This improvement originates from the applied voltages that facilitate the extraction of the photogenerated charges.

Responsivity ($R$), detectivity ($D^*$), and sensitivity ($S$) are key performance metrics of a photodetector, which we report for each device in Fig. 6(b)–(d). Under the same biasing conditions, p(C$_6$NDI-T) demonstrates the highest sensitivity as a photodetector, followed by P-90, gAIID-2FT, and BBL (Fig. 6(b)). However, since each device has a different $g_m$, which varies with the applied $V_{GS}$, it is fairer to evaluate sensitivity as a function of $V_{GS}$. Fig. 6(c) reveals that the devices exhibit a maximum peak sensitivity ($S_{max}$) at different biasing conditions. This finding suggests the flexibility to select a specific film and adjust the operating conditions to achieve the desired sensitivity level on demand.

We emphasize the significance of OECT $g_m$ in determining the sensitivity of the phototransistor. Despite gAIID-2FT demonstrating the largest change in OCP with light, its OECT has the lowest intrinsic $g_m$, resulting in the lowest sensitivity among the OPECTs studied. Fig. 6(d) shows the change in $R$ with respect to $V_{GS}$. Among the polymers studied, p(C$_6$NDI-T) demonstrates the highest responsivity, reaching 0.02 A W$^{-1}$, followed by BBL and gAIID-2FT. The $D^*$ follows the same trend (Fig. S22, ESI†). The exceptional responsivity of p(C$_6$NDI-T) OPECT can be attributed to the superior photosensitivity of this material and to the moderately high $g_m$ of its OECT. In contrast, although BBL exhibits the lowest photosensitivity, its OECT has a remarkably high $g_m$, making it the second-best performing OPECT. Similarly, gAIID-2FT demonstrates the
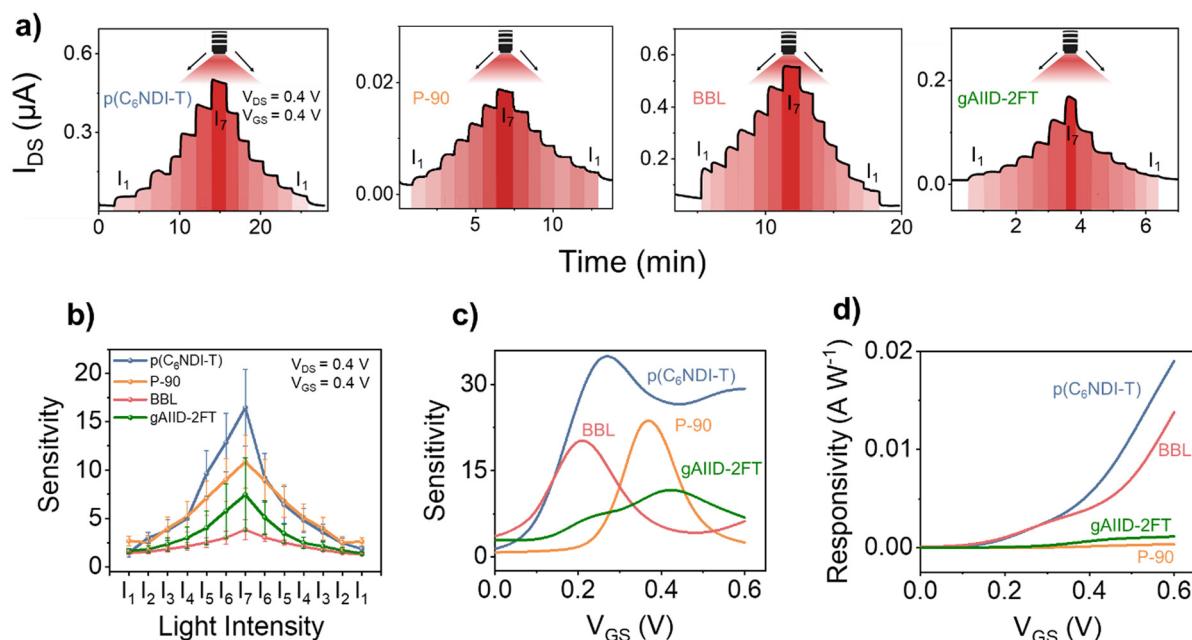


**Fig. 6** (a) The real-time current response of OPECTs to different light intensities, monitored at $V_{DS} = V_{GS} = 0.4$ V. The intensity of the light was gradually raised and then dropped. The intensity varied between 0.003 and 0.258 W cm$^{-2}$. The corresponding values of $I_1$, $I_2$, $I_3$, $I_4$, $I_5$, $I_6$, and $I_7$ are shown in Table S2 (ESI†). (b) Sensitivity of OPECTs to various light intensities. The data were reported at $V_{DS} = V_{GS} = 0.4$ V. The error bars were obtained from 4 OPECTs for each device. The sensitivity (c) and responsivity (d) of the OPECTs to 0.258 W cm$^{-2}$ deep red light as a function of $V_{GS}$. $V_{DS} = 0.4$ V.

highest photosensitivity, but its OECT's low $g_m$ results in the lowest overall performance compared to other OPECTs.

Table S6 (ESI†) summarizes the characteristics of all other aqueous electrolyte-gated OPECT devices. Notably, our p($C_6$NDI-T)-based device exhibits a remarkable 39-fold increase in transconductance when illuminated, implying that it can be 39 times more sensitive to a given analyte. Moreover, the p($C_6$NDI-T) OPECT demonstrates a 33-fold change in current, the highest among reported devices. This outstanding performance is attributed to the high photosensitivity of our organic mixed conductor and the unique transduction mechanism of the OPECT. In this mechanism, the device leverages not only the potential change at the gate electrode but also the light-induced reduction in impedance of the n-type material at the gate. This operational mode distinguishes our OPECT from other electrochemical photodetectors, resulting in exceptional voltage–current transduction performance.

## Conclusions

We developed aqueous electrolyte-gated organic photoelectro-chemical transistors (OPECTs) using a single n-type light-sensitive polymer film that conducts both ionic and electronic charges. By incorporating the polymer into the micron-scale channel and the gate of the OECT, we were able to streamline the fabrication process. Our investigation focused on quantifying the photosensitivity of n-type polymers by analyzing their photovoltage response. We observed that polymers with longer exciton lifetimes exhibited a greater change in electrochemical potential when exposed to light. Light exposure led to a downward shift in the electrochemical potential as well as a reduction in the impedance of the polymeric gate electrode, effectively enhancing the gating efficiency and doping the n-type channel. As a result, we achieved a single-component phototransistor that operates in aqueous electrolytes, with the current output scaling linearly and reversibly with light intensity. Our findings highlight the importance of high intrinsic photosensitivity for achieving a significant transconductance increase with light, which is critical for high signal-to-noise ratio sensing. A high OECT transconductance is also necessary to effectively transduce and amplify light-induced changes at the gate electrode, enabling the OPECT to function as a photodetector. This study not only provides insights into designing a single material for constructing high-performance OPECTs as photodetectors but also demonstrates their potential in biosensors, memory devices, and logic gates that utilize light as the input stimulus instead of or in addition to voltage.

## Author contributions

L. A. wrote the initial draft, fabricated the devices, performed all the experiments, and analyzed the data, except for TA spectroscopy, DIA spectroscopy, and TRTS experiments, which were performed and analyzed by C. E. P., N. A., and F. L. V. D. conducted the CV measurements for LUMO level determination and assisted L. A. in experimental design and analysis. W. S. assisted L. A. by conducting some of the response time experiments, stability experiments using the Ag/AgCl gate, and pulsing experiments with varying pulse lengths. S. G. and I. M. provided the p($C_6$NDI-T) and P-90, Y. W. and W. Y. provided gAIID-2FT, and M. A. and I. M. provided the P-75. S. I. designed the experiments, supervised the work, and revised the manuscript.

## Conflicts of interest

The authors declare no conflict of interest.

## Acknowledgements

## References

1 J. Rivnay, S. Inal, A. Salleo, R. M. Owens, M. Berggren and G. G. Malliaras, *Nat. Rev. Mater.*, 2018, **3**, 1.
2 A. Marks, S. Griggs, N. Gasparini and M. Moser, *Adv. Mater. Interfaces*, 2022, **9**, 2102039.
3 H. Shen, A. Abtahi, B. Lussem, B. W. Boudouris and J. Mei, *ACS Appl. Electron. Mater.*, 2021, **3**, 2434.
4 E. Macchia, R. A. Picca, K. Manoli, C. Di Franco, D. Blasi, L. Sarcina, N. Ditaranto, N. Cioffi, R. Österbacka and G. Scamarcio, *Mater. Horiz.*, 2020, **7**, 999.
5 D. Khodagholy, T. Doublet, P. Quilichini, M. Gurfinkel, P. Leleux, A. Ghestem, E. Ismailova, T. Hervé, S. Sanaur and C. Bernard, *Nat. Commun.*, 2013, **4**, 1575.
6 A. Koklu, S. Wustoni, K. Guo, R. Silva, L. Salvigni, A. Hama, E. Diaz-Galicia, M. Moser, A. Marks and I. McCulloch, *Adv. Mater.*, 2022, **34**, 2202972.
7 C.-J. Li, Y.-T. Xu, M.-J. Lu, Y.-M. Li, R. Ban, J. Hu, G. Gao, X.-Y. Dong, H. Zhou and P. Lin, *Biosens. Bioelectron.*, 2022, 114700.
8 L. Ding, Y. Liu, J. Lai, W. Zhu, C. Fan, N. Hao, J. Wei, J. Qian and K. Wang, *Adv. Funct. Mater.*, 2022, 2202735.
9 J. Hu, M.-J. Lu, F.-Z. Chen, H.-M. Jia, H. Zhou, K. Li, X. Zeng, W.-W. Zhao and P. Lin, *Adv. Funct. Mater.*, 2022, **32**, 2109046.
10 Z. Li, J. Hu, G. Gao, X.-N. Liu, J.-Q. Wu, Y.-T. Xu, H. Zhou, W.-W. Zhao, J.-J. Xu and H.-Y. Chen, *Sens. Diagn.*, 2022, **1**, 294.

11 J. Song, P. Lin, Y.-F. Ruan, W.-W. Zhao, W. Wei, J. Hu, S. Ke, X. Zeng, J.-J. Xu and H.-Y. Chen, *Adv. Healthcare Mater.*, 2018, **7**, 1800536.

12 Z. Li, Y.-T. Xu, J. Hu, X.-N. Liu, F.-Z. Chen, H.-M. Jia, H. Zhou, G. Chen, P. Lin and W.-W. Zhao, *Adv. Mater. Interfaces*, 2022, **9**, 2102040.

13 F. Corrado, U. Bruno, M. Prato, A. Carella, V. Criscuolo, A. Massaro, M. Pavone, A. B. Muñoz-García, S. Forti, C. Coletti, O. Bettucci and F. Santoro, *Nat. Commun.*, 2023, **14**, 6760.

14 G. Gao, J. Hu, Z. Li, Q. Xu, C.-S. Wang, H.-M. Jia, H. Zhou, P. Lin and W.-W. Zhao, *Biosens. Bioelectron.*, 2022, **209**, 114224.

15 M.-J. Lu, C.-J. Li, R. Ban, F.-Z. Chen, J. Hu, G. Gao, H. Zhou, P. Lin and W.-W. Zhao, *ACS Sens.*, 2022, 7, 2788.

16 G. Gao, J.-H. Chen, M.-J. Jing, J. Hu, Q. Xu, C.-S. Wang, H. Zhou, P. Lin, G. Chen and W.-W. Zhao, *Adv. Funct. Mater.*, 2023, 2300580.

17 Y.-T. Xu, Z. Li, C. Yuan, J.-Q. Wu, J. Hu, P. Lin, W.-W. Zhao, H.-Y. Chen and J.-J. Xu, *Adv. Opt. Mater.*, 2022, **10**, 2102687.

18 V. Druet, D. Ohayon, C. E. Petoukhoff, Y. Zhong, N. Alshehri, A. Koklu, P. D. Nayak, L. Salvigni, L. Almulla, J. Surgailis, S. Griggs, I. McCulloch, F. Laquai and S. Inal, *Nat. Commun.*, 2023, **14**, 5481.

19 A. Koklu, S. Wustoni, V.-E. Musteata, D. Ohayon, M. Moser, I. McCulloch, S. P. Nunes and S. Inal, *ACS Nano*, 2021, **15**, 8130.

20 A. Giovannitti, I. P. Maria, D. Hanifi, M. J. Donahue, D. Bryant, K. J. Barth, B. E. Makdah, A. Savva, D. Moia and M. Zetek, *Chem. Mater.*, 2018, **30**, 2945.

21 Y. Wang, G. Zhu, E. Zeglio, T. C. H. Castillo, S. Haseena, M. K. Ravva, S. Cong, J. Chen, L. Lan and Z. Li, *Chem. Mater.*, 2023, 2304103.

22 M. Alsufyani, M.-A. Stoeckel, X. Chen, K. Thorley, R. K. Hallani, Y. Puttisong, X. Ji, D. Meli, B. D. Paulsen, J. Strzalka, K. Regeta, C. Combe, H. Chen, J. Tian, J. Rivnay, S. Fabiano and I. McCulloch, *Angew. Chem., Int. Ed.*, 2022, **61**, e202113078.

23 M. Alsufyani, M.-A. Stoeckel, X. Chen, K. Thorley, R. K. Hallani, Y. Puttisong, X. Ji, D. Meli, B. D. Paulsen and J. Strzalka, *Angew. Chem.*, 2022, **134**, e202113078.

24 J. Surgailis, A. Savva, V. Druet, B. D. Paulsen, R. Wu, A. Hamidi-Sakr, D. Ohayon, G. Nikiforidis, X. Chen and I. McCulloch, *Adv. Funct. Mater.*, 2021, **31**, 2010165.

25 V. Druet, P. D. Nayak, A. Koklu, D. Ohayon, A. Hama, X. Chen, M. Moser, I. McCulloch and S. Inal, *Adv. Electron. Mater.*, 2022, **8**, 2200065.

26 J. Surgailis, A. Savva, V. Druet, B. D. Paulsen, R. Wu, A. Hamidi-Sakr, D. Ohayon, G. Nikiforidis, X. Chen and I. McCulloch, *Adv. Funct. Mater.*, 2021, **31**, 2010165.

27 D. Tsokkou, L. Peterhans, D. X. Cao, C.-K. Mai, G. C. Bazan, T.-Q. Nguyen and N. Banerji, *Adv. Funct. Mater.*, 2020, **30**, 1906148.

28 D. Tsokkou, C.-Y. Cheng, N. Krainova, S. Mukhopadhyay, N. C. Giebink and N. Banerji, *J. Phys. Chem. C*, 2021, **125**, 7086.

29 K. Chen, H. Hu, I. Song, H. B. Gobeze, W.-J. Lee, A. Abtahi, K. S. Schanze and J. Mei, *Nat. Photonics*, 2023, **17**, 629.